NANO LETTERS

Letter

pubs.acs.org/NanoLett

# In Situ Atomic Force Microscopy Tip-Induced Deformations and Raman Spectroscopy Characterization of Single-Wall Carbon Nanotubes

P. T. Araujo,[†,‡] N. M. Barbosa Neto,[†,§] H. Chacham,[†] S. S. Carara,[†] J. S. Soares,[†] A. D. Souza,[†] L. G. Cançado,[†] A. B. de Oliveira,[⊥] R. J. C. Batista,[⊥] E. Joselevich,[∥] M. S. Dresselhaus,[‡] and A. Jorio*[,†]

[†]Departamento de Física, Universidade Federal de Minas Gerais, Belo Horizonte, MG, 30123-970 Brazil

[‡]Department of Electrical Engineering and Computer Science, Massachusetts Institute of Technology, Cambridge, Massachusetts 02139-4307, United States

[§]Instituto de Física, *Universidade Federal de Uberlândia*, Uberlândia, MG, 38400-902 Brazil

[⊥]Departamento de Física, Universidade Federal de Ouro Preto, Campus Morro do Cruzeiro, Ouro Preto, MG, 35400-000 Brazil

[∥]Department of Materials and Interfaces, Weizmann Institute of Science, Rehovot, 76100, Israel

*S* *Supporting Information*

**ABSTRACT:** In this work, an atomic force microscope (AFM) is combined with a confocal Raman spectroscopy setup to follow in situ the evolution of the G-band feature of isolated single-wall carbon nanotubes (SWNTs) under transverse deformation. The SWNTs are pressed by a gold AFM tip against the substrate where they are sitting. From eight deformed SWNTs, five exhibit an overall decrease in the Raman signal intensity, while three exhibit vibrational changes related to the circumferential symmetry breaking. Our results reveal chirality dependent effects, which are averaged out in SWNT bundle measurements, including a previously elusive mode symmetry breaking that is here explored using molecular dynamics calculations.

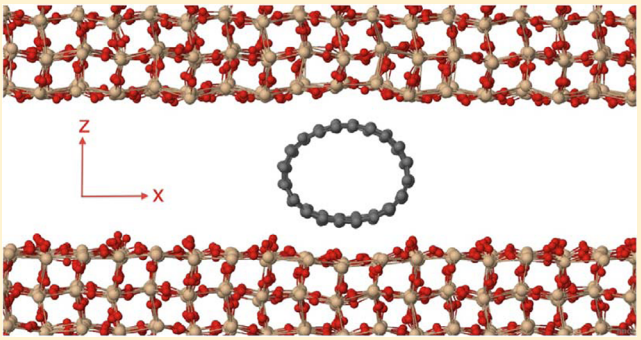


**KEYWORDS:** *Carbon nanotube, transverse deformation, Raman spectroscopy, molecular dynamics*

Single-wall carbon nanotubes (SWNTs) have received a great deal of attention because of their unusual properties and as a promising material for optical, electronic, and optoelectronic applications.[1,2] To achieve the stage of full technological applications, it is necessary to correlate the SWNT properties with environmental factors,[3−6] including external forces.[5,7−17] Uniaxial (along the tube-axis), torsional, and/or transverse (perpendicular to the tube axis) deformations are able to rehybridize atomic orbitals and may turn a semiconducting SWNT into a metallic SWNT.[6,16,18] Breaking symmetries and degeneracies in the SWNT phonon dispersion influences their transport properties.[1] The surrounding environment itself can compress the SWNTs, thereby affecting their properties.[5,19] The interaction of an isolated SWNT with a substrate on which it is sitting can also exhibit strong influences.[3,6,18,20,21]

Resonance Raman scattering (RRS) is a very powerful nondestructive technique, which can be used to reveal changes in SWNT properties.[22,23] In particular, the G band (tangential stretching modes) has been used to study environmental or intentionally induced structural changes.[1,22,23] More specifically, RRS has been largely used to study effects caused by strain, mostly focusing on the G-band behavior.[10−15] Most experiments were focused on SWNT bundles,[10,14,15,17] likely because of the lack of an appropriate experimental setup for isolated SWNT measurements. The effect of hydrostatic pressure on SWNT bundles has then been defined as an upshift in the G-band frequencies for low pressure values, followed by broadening and a further disappearance of the G-band signal when increasing pressure. Circumferential symmetry breaking (ovalization) and tube collapse are expected at higher pressure values, and these effects have been invocated to explain, respectively, the broadening and disappearance of the G-band signal, although a clear indication of those is still missing. Experiments on isolated SWNTs have also been performed, but dealing with uniaxial strain along the tube axis,[11,12] without addressing the effect of circumferential deformation.

Here, a home-built system that combines atomic force microscopy (AFM) with confocal Raman spectroscopy is used to follow in situ the evolution with applied transverse pressure

**Received:** April 30, 2012
**Revised:** June 12, 2012
**Published:** June 25, 2012

   dx.doi.org/10.1021/nl3016347 | *Nano Lett.* 2012, 12, 4110−4116

of the G-band feature in isolated SWNTs deposited on a substrate (see Figure 1a). SWNTs grown on quartz were used

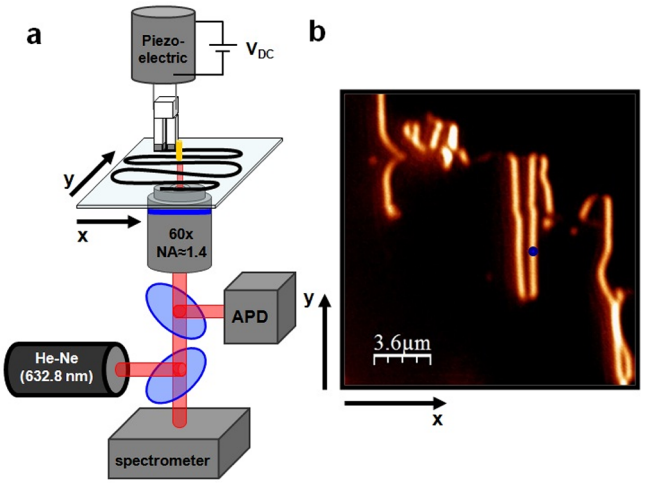


**Figure 1.** The experimental setup. (a) The system includes an *XY*-stage coupled to an inverted microscope, combined with an AFM system. The *XY*-stage allows for a raster scan of the sample which is illuminated from below, through an oil-immersion objective with high numerical aperture (NA = 1.4) and 60× magnification. The backscattered signal is sent to an avalanche photodiode detector (APD). For the 632.8 nm laser excitation used here, a 10 nm band-pass filter centered at 700 nm is placed in front of the APD to processes the scattered signal allowing us to image the G-band Raman feature intensity throughout the SWNT deposited on a quartz substrate, as shown in (b). A specific location in the SWNT [e.g., blue spot in (b)] can be selected, and local transverse pressures can be applied via the AFM tip, while Raman spectra are measured with a monochromator spectrometer equipped with a charged-coupled device camera.

(see refs[6,20,21] for sample details). Soares et al.[6,20] have shown that different SWNTs exhibit different levels of tube/substrate interaction, as evidenced by different levels of changes in the G band along the same SWNT. For our purpose here, we have chosen SWNTs with the smallest evidence for tube/substrate interaction, by monitoring and searching for small variations of the G band Raman signal all along the SWNTs.

Figure 1b shows the G-band image of a SWNT, obtained as described in the caption to Figure 1. Guided by this image, the Raman spectra of the G-band feature can be measured in a backscattering geometry at selected locations (e.g., the blue spot in Figure 1b). Transverse pressures can be applied using an AFM tip attached to a quartz tuning-fork monitored by a shear-force sensitive feedback mechanism (see Figure 1a).[24] The tip is first positioned over a previously characterized SWNT section and the feedback loop is deactivated, enabling the tip−sample distance to be exclusively controlled by the application of voltages to a piezo-electric element in which the tuning-fork is coupled (see Figure 1a). The experiments reported here were all obtained with AFM tips made of gold, by electrochemical etching of a 100 $\mu$m gold wire.[24] This brings in an important experimental aspect. Gold is a soft material, and one could argue that it would be better to perform the work with hard tips, for well-controlled pressure effects. However, several experiments were made with silicon and glass tips, and they were all unsuccessful, that is, no change has been observed in the SWNT G band spectra. The experiments with gold tips show some sort of effect, as we will report here. The reason why the gold tips work might be either due to a tip enhanced Raman spectroscopy (TERS) effect[24] or because the tip deformation is indeed needed, so that the tip can cover a larger SWNT segment under the ∼0.3 $\mu$m laser spot in the confocal Raman setup (usual tip radius after the experiment is ∼0.5 $\mu$m, as shown in the Supporting Information). Consequently, we have not performed multiple loading/unloading experiments and the pressure levels will be given here in arbitrary units. It is important to point out also the following: (i) TERS experiments on SWNTs have never shown the appearance of new peaks, but just the overall Raman intensity enhancement;[24] (ii) no radial breathing mode[23,24] has been observed in our measurements; (iii) the complete absence of the well-known disorder induced D band feature before, during and after our experiments guarantees that no damage (C−C bond break) is being induced on the tube walls.[25,26]

Our measurement was optimized to have both the incident and scattered light parallel to the SWNT axis, so that the spectrum is dominated by the two totally symmetric $A_{1g}$ modes.[22,23] In achiral SWNTs, these two components represent (i) the transverse optical (TO) component, where atomic vibrations are along the tube circumference (lower frequency $G^-$ peak in semiconducting SWNTs) and (ii) the longitudinal optical (LO) component, where the atomic vibrations are along the tube axis (higher frequency $G^+$ peak in semiconducting SWNTs).[22,23] In chiral SWNTs, these two components are not strictly along the two high symmetry directions, and the $G^+$ and $G^-$ peaks exhibit a mixed LO and TO nature with the degree of mixing depending on chiral angle.[22,23,27]

The experiment, as described above, was successful in eight physically distinct SWNTs. In five SWNTs (not shown here), the observed effect is just an overall decrease in the G band intensity, which almost vanishes for the largest applied pressure, but shows no change in the G band line shape (case 1). The intensity is recovered when retracting the tip, in a reversible process. We performed first-principles calculations for a carbon nanotube being compressed by Au slabs, and the calculations show a progressive broadening and disappearance of the DOS features of the isolated nanotube, as the nanotube is compressed (see Supporting Information). This is consistent with an increasing coupling between the nanotube electronic states and the gold surface states as the nanotube−Au distance is reduced, turning the one-dimensional nanotube electronic states into states with higher dimensionality. By "washing out" the one-dimensional Van Hove singularities, the unusually high optical absorption from this quasi-one-dimensional system is reduced. This effect is expected for any SWNT, independent of diameter and chiral angle.

The other three measurements show richer results. Besides the overall decrease in intensity when applying pressure, in two SWNTs an increase in the $G^+$−$G^-$ frequency splitting was observed (case 2), and the third SWNT exhibited a previously elusive fundamental symmetry breaking of the TO mode, observed here from the $G^-$ mode splitting in two peaks (case 3). Cases 2 and 3 will be discussed below.

For case 2, Figure 2 shows the G-band Raman profiles of an isolated SWNT sitting on quartz. The spectra were obtained at different levels of transverse pressure in a fixed SWNT location for both increasing (Figure 2a) and decreasing (Figure 2b) the pressure during the procedure of pressing the tube with the AFM gold tip. The G band was properly monitored in different locations along this SWNT, as indicated in Figure 2c. An overview of Figure 2a,b shows that the spectral changes


dx.doi.org/10.1021/nl3016347 | *Nano Lett.* 2012, 12, 4110−4116

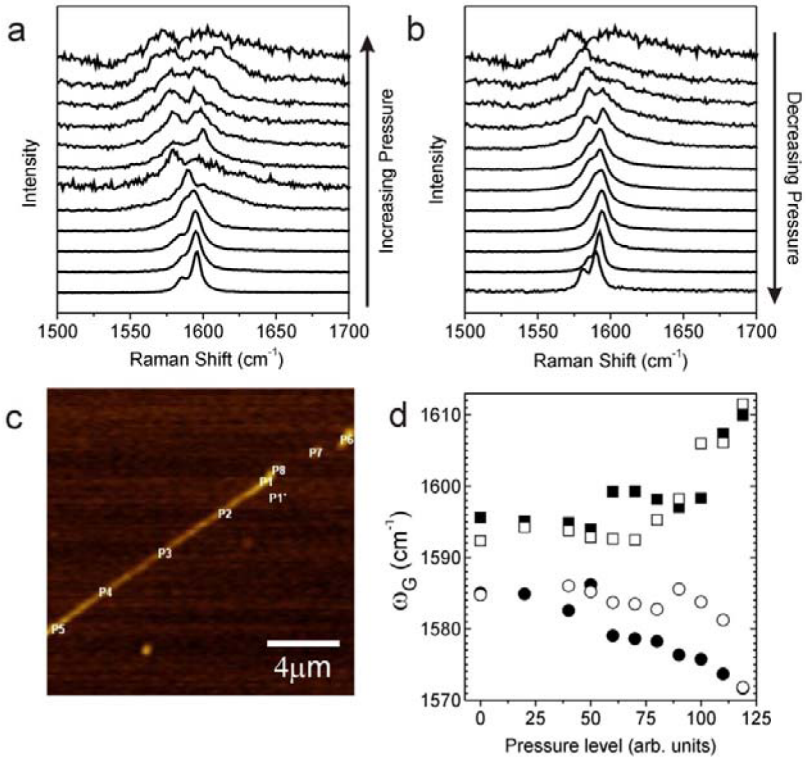


**Figure 2.** Evolution of the G band with applied pressure, the $G^+$–$G^-$ mode frequency splitting. (a) The level of pressure is being increased, as indicated by the arrow. (b) The level of pressure is being decreased, as indicated by the arrow. (c) The Raman image of the measured tube, showing different locations where the G band was monitored. (d) The G band frequency versus applied pressure; filled symbols stand for increasing and open symbols for decreasing pressure. Circles and squares stand for the $G^-$ and $G^+$ peaks, respectively.

observed are reversible. The pressure-induced frequency behavior for the two totally symmetric G band modes is shown in Figure 2d, obtained by fitting the spectra with two Lorentzian lines. The $G^+$–$G^-$ frequency splitting and the broadening of both peaks are observed. Similar behavior was observed in another physically distinct SWNT, although for this SWNT (not shown here) the process was not fully reversible when the tip was retracted.

For case 3, Figure 3a shows Raman G-band profiles obtained from another SWNT under a new AFM tip pressing experiment. Here we display only the three extreme situations, which means (i) before applying pressure (top spectrum), (ii) during the strongest applied pressure (middle spectrum), and (iii) after retracting the tip (bottom spectrum). In this case, a new mode appears related to the tube deformation (see middle spectrum in Figure 3a as compared to the top spectrum). The broad frequency range in Figure 3a shows the complete absence of the D band, even when the tip is pressing the tube.

Before going deeper into the deformation effect, it is important to address the G-band line shape in Figure 3a as compared to Figure 2a,b. Both are characteristic of semiconducting SWNTs, based on the small peak widths.[22,23] However, the relative intensities of the $G^-$ and the $G^+$ peaks are opposite from one another (compare bottom spectra in Figures 2a,b with the top spectrum in Figure 3a). The intensity ratio between the $G^+$ and $G^-$ peaks is known to be determined by the SWNT chiral angle.[22,23,28] Case 2 indicates a chiral angle near 10–15°, while case 3 indicates a chiral angle near 30°, and this is known to affect the LO/TO nature of the G band peaks.[27,29] According to recent calculations,[29] SWNTs with chiral angles near 30° (also near 0°) show a well-defined LO/TO nature for the two G band modes, while for SWNTs with a chiral angle near 10–15°, both peaks have a mixed LO/TO nature. As discussed below, this is why case 2 shows the $G^+/G^-$ splitting (i.e., no LO/TO nature and both modes are affected), while case 3 shows no change on the $G^+$ (LO) peak, and the splitting on the $G^-$ (TO) peak (i.e., well-defined LO/TO nature and only TO mode is affected).

Now back to the pressure effects, Figure 3a shows the appearance of a new feature in the G-band profile when applying pressure, rather than just the splitting of the $G^+$ and $G^-$ modes, as observed in Figure 2. Figure 3b plots the evolution of the frequency shifts for the G band peaks for all different levels of pressure as obtained by fitting the spectra with up to three Lorentzian peaks. The horizontal axis in Figure 3b is numbered from 0 to 10, and the experiment runs from the left to the right, which means increasing the pressure from the lowest to the highest value (filled symbols), then decreasing the pressure back to 0 (open symbols). From Figure 3b it is clear that the lower frequency $G^-$ (TO) mode splits in two peaks ($TO_1$ and $TO_2$) when pressure is applied to this SWNT. The $TO_1$–$TO_2$ splitting increases when the applied pressure increases. When slowly retracting the tip, the splitting decreases but the SWNT does not fully recover the degenerate state observed before the experiment started (compare bottom and top spectra in Figure 3a). Therefore, the process is not fully reversible, suggesting that the SWNT remains slightly deformed after retracting the tip. On the other hand, the $G^+$ (LO) component remains basically unchanged during the entire pressure application process.

Considering the TO versus LO nature of the totally symmetric G band modes, it is natural that the TO mode


dx.doi.org/10.1021/nl3016347 | Nano Lett. 2012, 12, 4110–4116

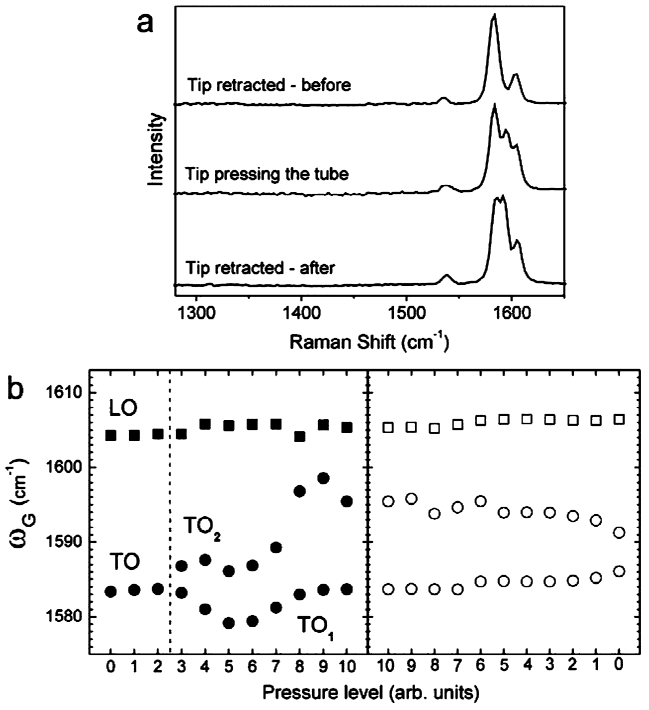


**Figure 3.** Evolution of the G band with applied pressure, the $G^-$ (TO) mode frequency splitting. (a) G-band profiles before applying pressure (top), during the strongest pressure level (middle) and after retracting the tip (bottom). (b) G-band frequencies acquired for different levels of transversal pressure. The data are numbered in the *X* axis from 0 to 10, which represents the levels of pressure, from the lowest to the highest level, respectively. From left to right, the pressure is being increased (0 to 10, filled symbols) and then decreased (from 10 to 0, open symbols). The $G^-$ (TO) mode splits into two peaks ($TO_1$ and $TO_2$) when pressure is applied (circles). The vertical dashed line shows the pressure level where the symmetry breaking occurs.

will be sensitive to changes in the SWNT curvature, while the LO will not. This curvature effect naturally appears in SWNTs with different diameters, where the TO mode frequency is softened with decreasing tube diameter, while the LO mode frequency remains unchanged.[22,23] The splitting of the TO mode suggests the breaking of the circumferential tube symmetry and the localization of vibrations at two different tube segments, as described below.

Molecular dynamics simulations are used here to elucidate the effect we observe in Figure 3. A view of the region of the unit cell near a compressed nanotube is shown in Figure 4. The cell was chosen to make the tube and slab commensurable along the tube axis ($y$) direction, so that no strain is imposed along the tube axis due to the cell periodicity. The computational details of the molecular dynamics simulation and the empirical potentials used are given in the Methods section.

After an initial thermalization procedure (see Methods section), the velocity autocorrelation function of the nanotube carbon atoms between a time $t_0$ and a later time $t$ is calculated as

$$f(t) = \frac{1}{N}\sum_{i=1}^{N} \vec{v}(t_0)\cdot\vec{v}(t) \qquad (1)$$

with the summation running over the $N$ carbon atoms. The phonon density of states (DOS) of the nanotube is then

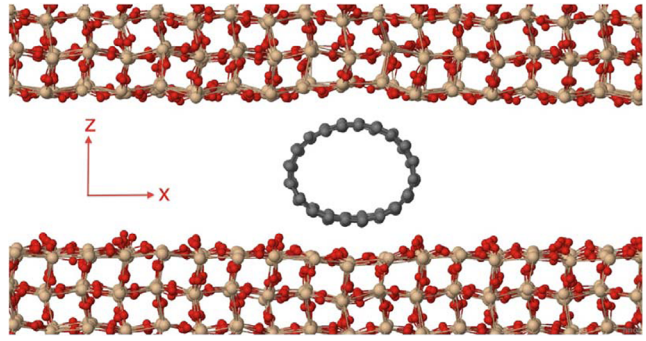


**Figure 4.** Cross-sectional view of a (10,0) nanotube compressed between two identical $SiO_2$ blocks, as used in the molecular dynamics simulations, for a radial compressive strain $s$ = 0.162. The $x$ and $z$ directions of the cell coordinate system are indicated. The $y$ is the tube axis direction.

calculated as the Fourier transform of $f(t)$, labeled by $F(\omega)$. The projected phonon DOS can also be defined from the $f_x$, $f_y$, and $f_z$ components of the velocity autocorrelation function, corresponding to the $x$, $y$, and $z$ components of the internal product in eq 1. Since $y$ is the tube axis direction, the $f_y$ component leads to a DOS projected onto the longitudinal modes, while the $f_x + f_z$ component leads to a DOS projected on transverse modes. They can be separated spectrally because the $f_y$ components appear at higher frequencies, as expected for the SWNT LO modes.

Figure 5 shows the projected density of states resulting from (i) the $f_x$ components in the frequency window corresponding

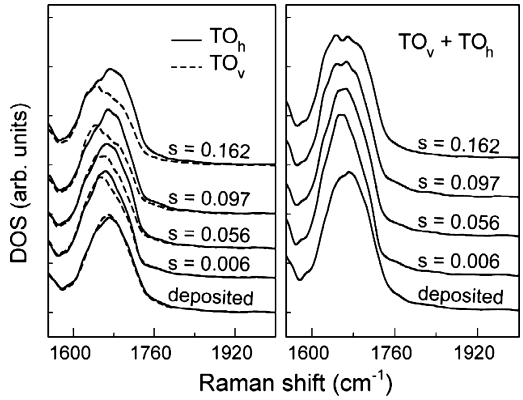


**Figure 5.** The DOS calculated for a (10, 0) nanotube in the frequency region of the transverse optical (TO) modes for several values of compressive strain $s$. In the left panel, $TO_h$ refers to vibrations along the horizontal ($x$ in Figure 4) direction, while component $TO_v$ refers to vibrations along the vertical ($z$ in Figure 4) direction. The DOS for a nanotube deposited on a quartz surface is also shown (labeled "deposited" in the figure). The right panel shows the sum of $TO_h$ plus $TO_v$.

to transverse optical (TO) modes with vibrations along the horizontal ($x$) direction (with respect to the surface), and we will refer to that as the $TO_h$ density of states; (ii) the $f_z$ components in the frequency window corresponding to transverse optical (TO) modes with vibrations along the vertical ($z$) direction, and we will refer to that as the $TO_v$ density of states. The progressive degree of radial deformation of the tube is measured by the radial compressive strain $s = 1 -$


dx.doi.org/10.1021/nl3016347 | *Nano Lett.* 2012, 12, 4110–4116

$h/D$, where $h$ is the compressed diameter along the vertical direction and $D$ is the diameter of the isolated nanotube.[18]

In a calculation for an isolated nanotube (without substrate, not shown in Figure 5), the $TO_h$ and the $TO_v$ densities of states are identical due to the symmetry of the nanotube. The left panel of Figure 5 shows that the $TO_h$−$TO_v$ degeneracy is progressively lifted as the symmetry of the nanotube is broken, first by being deposited at the surface (see "deposited" in Figure 5), and further by being compressed by the surface above it (increasing $s$ values in Figure 5). The tube-substrate interaction is not strong enough to make the symmetry-breaking to be a measurable effect. The splitting of the $TO_h$ and the $TO_v$ peaks is such that the $TO_v$ peak shifts to lower frequencies, relative to the $TO_h$ peak, as the nanotube is flattened. This is indeed expected since $TO_v$ is localized along the most distorted tube segments, and the larger the tube curvature, the lower G band frequency.[22,23] In the case studied here, the $TO_h$−$TO_v$ splitting results in a double-peak structure of the total TO density of states for nanotube strains on the order of $s$ = 0.1 or more, as shown in the right panel of Figure 5. Although we are not looking at the Raman active zone center phonons, this double-peak structure clearly demonstrates the splitting of the transverse optical vibrations, and it can be associated with the $TO_1$ and $TO_2$ features observed in the Raman spectra of the compressed nanotubes discussed in Figure 3.

It is interesting to compare the results reported here with those obtained with SWNT bundles. The present results are based on a transverse deformation nanomanipulation procedure, while in bundles the results are based on hydrostatic pressure.[10,14,15,17] First of all, the decrease in Raman intensity when pressure is applied is always observed in both isolated and bundles SWNTs due to the Van Hove singularity "wash out" (see Supporting Information). Second, in SWNT bundles both $G^+$ and $G^-$ show an upshift in frequency, expected for hydrostatic pressures, since the C−C distance is decreased. In our experiment, this is not expected since no symmetrical hydrostatic pressure is applied. Our results show that at the single nanotube level the symmetry breaking effects depend on tube chiral angle, so that different G-band frequency behaviors are observed for different SWNTs. This dependence is here related to the fact that the TO versus LO nature of the vibrational modes in SWNTs depend on the SWNT chiral angle.[22,23,27,29] These results are averaged out in SWNT bundle measurements. From another perspective, our results confirm the circumferential symmetry-breaking effect, which is invocated to explain the high hydrostatic pressure effects observed in SWNT bundles. More experimental and theoretical works are needed to address the distinction between ovalization and tube collapse, which may be related to the reversible versus irreversible behaviors shown here.

In summary, a home-built setup combining atomic force microscopy (AFM) with confocal Raman spectroscopy is used to simultaneously follow in situ the evolution of the G-band feature in isolated SWNTs deposited on a quartz substrate, while changing the transverse pressure applied to this system via a gold AFM tip. A previously elusive and fundamental symmetry-breaking effect was observed for the totally symmetric TO G-band mode, which exhibits two distinct Raman-active features with increasing applied pressure, while the LO component is kept unchanged. This experimental finding is consistent with molecular dynamics simulations for a transversely compressed achiral nanotube, which shows the appearance of a double-peaked TO band due to the circumferential symmetry breaking of the compressed nanotube. Two different SWNTs show another behavior, that is, a $G^+/G^-$ (mixed LO/TO) frequency splitting followed by peak broadening. Finally, measurements performed on five other SWNTs show a reduction of the G band intensity with no change in the G line shape. From the G band profiles prior to the pressure applications, the tubes measured here exhibit different chiral angles, and this explains the different G-band behaviors, since the TO versus LO nature of the vibrational modes in SWNTs indeed depends on chirality. Our work thus provides evidence for the richness of transverse deformation at the isolated SWNT level, while maintaining consistency with averaged results on SWNT bundle measurements.

**Methods.** *Molecular Dynamics Calculations.* The systems considered for simulations are composed of a (10,0) SWNT, consisting of 520 atoms with a length of 55 Å along the $y$-direction, deposited over a crystalline $SiO_2$ block or between two identical $SiO_2$ blocks. Each block is composed of 8520 atoms whose dimensions are 77, 55, and 30 Å along $x$, $y$, and $z$ directions, respectively. Periodic boundary conditions were applied in the $x$ and $y$ directions of the simulation box, whereas its $z$-component was kept with a finite length of 92.6 Å. A time step of $\delta t$ = 0.0005 ps was used in conjunction with the Nosé−Hoover thermostat[30] and barostat[31] for controlling the temperature and pressure. Only the $x$ and $y$ directions of the simulation box were allowed to fluctuate for fixing the pressure at 1.0 bar in all simulation runs. Yet, 1440 atoms localized in the bottom of the lower substrate and 1560 atoms in the top of the upper substrate (roughly two crystalline layers in both substrates) were kept with force zero in all runs.

The C, Si, and O atoms were modeled classically using the molecular dynamics package LAMMPS[32] with interaction potentials given as follows: (i) for the C−C interaction, we used the adaptive intermolecular reactive empirical bond order (AIREBO) potential[33] derived from the second-generation Brenner potential.[34] The AIREBO potential is known to accurately reproduce the phonon DOS of carbon nanotubes.[35] (ii) For modeling the crystalline $SiO_2$ substrate (Si−Si, Si−O, and O−O interactions), we applied the Tersoff[36] potential with parameters given by Munetoh et al.[37] This potential is suitable for simulations of large systems, giving structural parameters, density, and cohesive energy for silica polymorphs in excellent agreement with both experimental data and ab initio calculations.[37] (iii) Regarding the nanotube−quartz interaction, that is, C−Si and C−O interactions, we followed the same strategy used by Ong and Pop,[35] where the correct description of the phonon DOS of the system is of crucial importance. For both the C−Si and C−O interactions, we used the well-known 12-6 Lennard-Jones (LJ) pair potential,[38] which depends on the interatomic distance $r$ between atoms $i$ and $j$. It may be written as

$$U_{ij}(\mathrm{r}) = 4\varepsilon_{ij}\left[\left(\frac{\sigma_{ij}}{r}\right)^{12} - \left(\frac{\sigma_{ij}}{r}\right)^{6}\right] \quad (2)$$

where $\sigma_{ij}$ is the effective collision (center-to-center) distance and $\varepsilon_{ij}$ is the energy strength, between atoms $i$ and $j$. The parameters used in our simulations were[35] $\varepsilon_{C-Si}$ = 8.909 meV, $\varepsilon_{C-O}$ = 3.442 meV, $\sigma_{C-Si}$ = 3.326 Å, and $\sigma_{C-O}$ = 3.001 Å. The cutoff distance for both C−Si and C−O cases was set to 10.0 Å. Before the production stage, the nanotube−$SiO_2$ compounds were annealed as follows. First, the temperature was linearly raised from $T$ = 3 to 300 K in 250 ps. After that, the systems


dx.doi.org/10.1021/nl3016347 | Nano Lett. 2012, 12, 4110−4116

were left to equilibrate during further 250 ps with $T$ = 300 K. Next, in the production stage the velocities of the C atoms were collected at intervals of 10 steps (or 0.005 ps) during 700 ps at $T$ = 300 K. The velocity autocorrelation function of carbon atoms between a time $t_0$ and a later time $t$ was then calculated as described previously in this paper with the summation running over the $N$ carbon atoms. For obtaining the phonon DOS of the tube we performed the fast Fourier transform of $f(t)$ using the Blackman window function[39] over 131 072 data points among those 140 000 collected in the production stage.

## ■ ASSOCIATED CONTENT

### Ⓢ Supporting Information

Description of the gold tips used to perform the experimental work, before and after the experiment, and the results from first principles calculations of a SWNT compressed between two gold slabs, showing the "wash out" of the one-dimensional van Hove singularities. This material is available free of charge via the Internet at http://pubs.acs.org.

## ■ AUTHOR INFORMATION

### Corresponding Author

*E-mail: adojorio@fisica.ufmg.br.

### Notes

The authors declare no competing financial interest.

## ■ ACKNOWLEDGMENTS

The authors thank A. G. Cano Marquéz and J. Ribeiro-Soares for technical assistance, A. G. Souza Filho for very important input, and L. M. Malard, D. L. Mafra, and M. S. C. Mazzoni for critical reading of the manuscript. A.B.O. is thankful to Zhun-Yong Ong for valuable discussions regarding the molecular dynamics model. This work was supported by Rede Brasileira de Pesquisa e Instrumentação em Nano-Espectroscopia Óptica and INCT em Nanomateriais de Carbono (CNPq/MCTI) and FAPEMIG (PPM and Pronex BioNC grants).

## ■ REFERENCES

(1) Jorio, A.; Dresselhaus, G.; Dresselhaus, M. S. *Carbon Nanotubes: Advanced Topics in the Synthesis, Structure, Properties and Applications*; Springer-Verlag: Berlin, 2008.

(2) Avouris, Ph.; Chen, Z.; Pereibenos, V. Carbon-based electronics. *Nat. Nanotechnol.* **2007**, *2*, 605−615.

(3) Hertel, T.; Walkup, R. E.; Avouris, Ph. Deformation of carbon nanotubes by surface van der Waals forces. *Phys. Rev. B* **1998**, *58*, 13870−13873.

(4) Thomsem, C.; Reich, S.; Goni, A. R.; Jantoljok, H.; Rafailov, P. M.; Loa, I.; Syassen, K.; Journet, C.; Bernier, P. Intermolecular interaction in carbon nanotube ropes. *Phys. Status. Solidi B* **1999**, *215*, 435.

(5) Araujo, P. T.; Maciel, I. O.; Pesce, P. B. C.; Pimenta, M. A.; Doorn, S. K.; Qian, H.; Hartschuh, A.; Steiner, M.; Grigorian, L.; Hata, K.; Jorio, A. Nature of the constant factor in the relation between radial breathing mode frequency and tube diameter for single-wall carbon nanotubes. *Phys. Rev. B* **2008**, *77*, 241403(R).

(6) Soares, J. S.; Barboza, A. P. M.; Araujo, P. T.; Neto, N. M. B.; Nakabayashi, D.; Shadmi, N.; Yarden, T. S.; Ismach, A.; Geblinger, N.; Joselevich, E.; Vilani, C.; Cançado, L. G.; Novotny, L.; Dresselhaus, G.; Dresselhaus, M. S.; Neves, B. R. A.; Mazzoni, M. S. C.; Jorio, A. Modulating the Electronic Properties along Carbon Nanotubes via Tube-Substrate Interaction. *Nano Lett.* **2010**, *10*, 5043−5048.

(7) Zhang, P.; Lammert, P. E.; Crespi, V. H. Plastic Deformations of Carbon Nanotubes. *Phys. Rev. Lett.* **1998**, *81*, 5346−5350.

(8) Tombler, T. W.; Zhou, C.; Alexseyev, L.; Kong, J.; Dai, H.; Liu, L.; Jayanthi, C. S.; Tang, M.; Wu, S. Y.. Reversible electromechanical characteristics of carbon nanotubes under local-probe manipulation. *Nature* **2000**, *405*, 767−769.

(9) Peters, M. J.; McNeil, L. E.; Ping, Lu, J.; Kahn, D. Structural phase transition in carbon nanotube bundles under pressure. *Phys. Rev. B* **2000**, *61*, 5939−5944.

(10) Reich, S.; Thomsen, C.; Ordejón, P. Elastic properties of carbon nanotubes under hydrostatic pressure. *Phys. Rev. B* **2002**, *65*, 153407.

(11) Cronin, S. B.; Swan, A. K.; Ünlü, M. S.; Goldberg, B. B.; Dresselhaus, M. S.; Tinkham, M. Measuring the uniaxial strain of individual single-wall carbon nanotubes: resonance Raman spectra of atomic-force-microscope modified single-wall nanotubes. *Phys. Rev. Lett.* **2004**, *93*, 167401−167405.

(12) Gao, B.; Lai, J.; Xi, L.; Zhang, L.; Liu, Z. Chirality-Dependent Raman Frequency Variation of Single-Walled Carbon Nanotubes under Uniaxial Strain. *J. Phys. Chem. C* **2008**, *112* (51), 20123−20125.

(13) Souza Filho, A. G.; Kobayashi, N.; Jiang, J.; Grüneis, A.; Saito, R.; Cronin, S. B.; Mendes Filho, J.; Samsonidze, Ge. G.; Dresselhaus, G.; Dresselhaus, M. S. Strain-induced interference effects on the resonance Raman cross section of carbon nanotubes. *Phys. Rev. Lett.* **2005**, *95*, 217403−217407.

(14) Yang, X.; Wu, G.; Dong, J. Structural transformations of double-wall carbon nanotubes bundle under hydrostatic pressure. *Appl. Phys. Lett.* **2006**, *89*, 113101−113103.

(15) Yao, M.; Wang, Z.; Liu, B.; Zou, Y.; Yu, S.; Lin, W.; Hou, Y.; Pan, S.; Jin, M.; Zou, B.; Cui, T.; Zou, G.; Sundqvist, B. Raman signature to identify the structural transition of single wall carbon nanotubes under high pressure. *Phys. Rev. B* **2008**, *78* (20), 205411.

(16) Barboza, A. P. M.; Gomes, A. P.; Archanjo, B. S.; Araujo, P. T.; Jorio, A.; Ferlauto, A. S.; Mazzoni, M. S. C.; Chacham, H.; Neves, B. R. A. Deformation induced semiconductor-metal transition in single wall carbon nanotubes probed by electric force microscopy. *Phys. Rev. Lett.* **2008**, *100*, 256804−256808.

(17) Aguiar, A. L.; Barros, E. B.; Capaz, R. B.; Souza Filho, A. G.; Freire, P. T. C.; Mendes Filho, J.; Machon, D.; Caillier, Ch.; Kim, Y. A.; Muramatsu, H.; Endo, M.; San-Miguel, A. Pressure-induced collapse in double-walled carbon nanotubes: Chemical and mechanical screening effects. *J. Phys. Chem. C* **2011**, *115*, 5378−5384.

(18) Mazzoni, M. S. C.; Chacham, H. Bandgap closure of a flattened semiconductor carbon nanotube: a first-principles study. *Appl. Phys. Lett.* **2000**, *76*, 1561−1564.

(19) Araujo, P. T.; Fantini, C.; Lucchese, M. M.; Dresselhaus, M. S.; Jorio, A. The effect of environment on the radial breathing mode of supergrowth single wall carbon nanotubes. *Appl. Phys. Lett.* **2009**, *95*, 261902−26195.

(20) Soares, J. S.; Jorio, A. Study of Carbon Nanotube-Substrate Interaction. *J. Nanotechnol.* **2012**, Article ID 512738.

(21) Geblinger, N.; Ismach, A.; Joselevich, E. Self-organized nanotube serpentines. *Nat. Nanotechnol.* **2008**, *3*, 195−200.

(22) Saito, R.; Hofmann, M.; Dresselhaus, G.; Jorio, A.; Dresselhaus, M. S. Raman spectroscopy of graphene and carbon nanotubes. *Adv. Phys.* **2011**, *60* (3), 413−550.

(23) Jorio, A.; Dresselhaus, M. S.; Saito, R.; Dresselhaus, G. *Raman Spectroscopy in Graphene Related Systems*; Wiley-VCH: Weinheim, 2011.

(24) Cançado, L. G.; Hartschuh, A.; Novotny, L. Tip-enhanced Raman spectroscopy of carbon nanotubes. *J. Raman Spectrosc.* **2009**, *40*, 1420−1426.

(25) Archanjo, B. S.; Maciel, I. O.; Martins Ferreira, E. H.; Peripolli, S. B.; Damasceno, J. C.; Achete, C. A.; Jorio, A. Ion beam nanopatterning and micro-Raman spectroscopy analysis on HOPG for testing FIB performances. *Ultramicroscopy* **2011**, *111* (8), 1338−1342.

(26) Maciel, I. O.; Anderson, N.; Pimenta, M. A.; Hartschuh, A.; Qian, H.; Terrones, M.; Terrones, H.; Campos-Delgado, J.; Rao, A. M.; Novotny, L.; Jorio, A. Electron and phonon renormalization near charged defects in carbon nanotubes. *Nat. Mater.* **2008**, *7*, 878−883.

(27) Reich, S.; Thomsen, C.; Ordejón, P. Phonon eigenvectors of chiral nanotubes. *Phys. Rev. B* **2001**, *64*, 195416.

(28) Saito, R.; Jorio, A.; Hafner, J. H.; Lieber, C. M.; Hunter, M.; McClure, T.; Dresselhaus, G.; Dresselhaus, M. S. Chirality-dependent G-band Raman intensity of carbon nanotubes. *Phys. Rev. B* **2001**, *64*, 085312.
(29) Park, J. S.; Sasaki, K.; Saito, R.; Izumida, W.; Kalbac, M.; Farhat, H.; Dresselhaus, G.; Dresselhaus, M. S. Fermi energy dependence of the G-band resonance Raman spectra of single-wall carbon nanotubes. *Phys. Rev. B* **2009**, *80*, 081402(R).
(30) Hoover, W. G. Canonical dynamics: Equilibrium phase-space distributions. *Phys. Rev. A* **1985**, *31*, 1695−1697.
(31) Hoover, W. G. Constant-pressure equations of motion. *Phys. Rev. A* **1986**, *34*, 2499−2500.
(32) Plimpton, S. J. Fast Parallel Algorithms for Short-Range Molecular Dynamics. *J. Comput. Phys.* **1995**, *117*, 1−19.
(33) Stuart, S. J.; Tutein, A. B.; Harrison, J. A. A reactive potential for hydrocarbons with intermolecular interactions. *J. Chem. Phys.* **2000**, *112*, 6472−6487.
(34) Brenner, D. W. Empirical potential for hydrocarbons for use in simulating the chemical vapor deposition of diamond films. *Phys. Rev. B* **1990**, *42*, 9458−9471.
(35) Ong, Z.-Y.; Pop, E. Molecular dynamics simulation of thermal boundary conductance between carbon nanotubes and $SiO_2$. *Phys. Rev. B* **2010**, *81*, 155408−155415.
(36) Tersoff, J. New empirical approach for the structure and energy of covalent systems. *Phys. Rev. B* **1988**, 6991−7000.
(37) Munetoh, S.; Motooka, T.; Moriguchi, K.; Shintani, A. Interatomic potential for Si−O systems using Tersoff parameterization. *Comput. Mater. Sci.* **2007**, *39*, 334−339.
(38) Jones, J. E. On the determination of molecular Fields. II. From the equation of state of a gas. *Proc. R. Soc. London, Ser. A* **1924**, *106*, 463−477.
(39) Harris, J. F. On the use of windows for harmonic analysis with the discrete Fourier transform. *Proc. IEEE* **1978**, *66*, 51−83.